Persistence and Stochastic Periodicity in the Intensity Dynamics of a Fiber Laser During the Transition to Optical Turbulence

Laura Carpi[1] and Cristina Masoller[2,*]

[1] *Programa de Pós-Graduação em Modelagem Matemática e Computacional, PPGMMC, Centro Federal de Educação Tecnológica de Minas Gerais, CEFET-MG. Av. Amazonas, 7675. 30510-000. Belo Horizonte, MG, Brazil*

[2] *Departament de Fisica, Universitat Politecnica de Catalunya, Colom 11, ES-08222 Terrassa, Barcelona, Spain*

Many natural systems display transitions among different dynamical regimes, which are difficult to identify when the data is noisy and high dimensional. A technologically relevant example is a fiber laser, which can display complex dynamical behaviors that involve nonlinear interactions of millions of cavity modes. Here we study the laminar–turbulence transition that occurs when the laser pump power is increased. By applying various data analysis tools to empirical intensity time series we characterize their persistence and demonstrate that at the transition temporal correlations can be precisely represented by a surprisingly simple model.

PACS numbers: 89.75.-k; 05.45.Tp; 42.55.Wd; 42.60.Mi

Fibre lasers are technologically relevant laser systems that can display complex spatio-temporal dynamics which involve nonlinear interactions of a huge number of cavity modes [1–3]. The transition to "optical turbulence" (in analogy with the laminar-turbulence transition in hydrodynamic) as the laser pump power is increased has received attention [4] and experimental observations of spatio-temporal dynamical regimes have yield new light into the rich underlying nonlinear physics [5, 6]. Long temporal correlations from one round-trip to another have been identified for various pump powers, and during the laminar-turbulence transition, temporal correlations with much shorter time scales have also been detected [7].

In [7] temporal correlations were investigated by using the horizontal visibility graph (HVG) [8], which is a method that maps a time series into a graph. Each data point in the empirical intensity time series, $\{I_1 \dots I_N\}$, is considered a node, and any two nodes, I_i and I_j, are connected by a link if there is "horizontal visibility" between them: $I_i > I_n$ and $I_j > I_n$ for all $i < n < j$. In this way the resulting graph keeps information about the temporal ordering of the data points in the sequence. The graph was then characterized by the degree distribution, $P(k)$, that gives the probability that a node (i.e., a data point I_i) has k links. Specifically, Shannon entropy computed from $P(k)$, $S[P]$ (referred to as HVG entropy) was computed for various laser pump powers. When the intensity time series were pre-processed such that only the intensity peaks higher than a threshold were analyzed, a sharp decrease of the HVG entropy was detected at the transition. In contrast, the HVG entropy decreased smoothly when all the data points were analyzed.

Here we use various data analysis tools to characterize the intensity dynamics at the transition. Examples of intensity time traces and the corresponding Fourier spectra are shown in Fig. 1. The experimental setup and datasets are described in [7]: the laser is a Raman fiber (normal dispersion) of 1 km placed between two fiber Bragg gratings acting as cavity mirrors; the pump power is varied from below to above the transition (which occurs for 0.9 W), and for each pump power a time series with 5×10^7 data points was recorded, with resolution $dt = 0.0125$ ns. At the transition noisy oscillations are seen with a periodicity of about 2.5 ns, while in the broadband power spectrum there is a narrow peak at 0.4 GHz. As it will be shown latter, the appearance of this noisy periodicity at the transition can be understood in terms of a surprisingly simple model.

To investigate the intensity dynamics we compare the empirical time series with synthetic series generated by stochastic processes with known properties. In the HVG approach this can be done by fitting the degree distribution to an exponential, $P(k) \propto \exp(-\lambda k)$, and then comparing the values of λ obtained from empirical and synthetic data. It has been conjectured [9] that λ unveils a chaotic process if $\lambda < \ln(3/2)$, an uncorrelated stochastic process if $\lambda = \ln(3/2) = 0.405$ and a correlated stochastic process if $\lambda > \ln(3/2)$. An exception of this conjecture is fractional Gaussian noise (fGn) that, with $\lambda < 0.406$, invades the chaotic region [10].

We chose to compare with synthetic data generated with fractional Brownian motion (fBm) because it models turbulent systems [11, 12]. fBm is a family of processes, $\mathbf{B}^{\mathcal{H}}(t)$, which is Gaussian, self-similar and endowed with stationary increments. fBm has controllable memory that can be tuned by the Hurst exponent $\mathcal{H}$, defining two distinct regions in the interval $0 < \mathcal{H} < 1$: when $\mathcal{H} > 0.5$ consecutive increments tend to have the same sign so that the process is *persistent*; in contrast, when $\mathcal{H} < 0.5$ consecutive increments are more likely to have opposite signs, so that the process is *anti-persistent*. When $\mathcal{H} = 0.5$, the process correspond to the memory-less Brownian motion for which

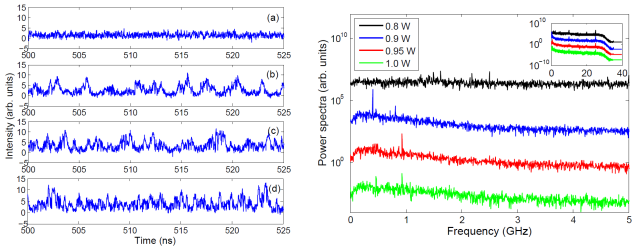

FIG. 1. Intensity time series and power spectra (separated vertically for clarity) below, during, and above the transition. The laser pump power is: (a) 0.8 W, (b) 0.9 W, (c) 0.95 W and (d) 1.0 W. In the power spectrum at the transition (blue line) there is a narrow peak at ∼0.4 GHz, while for a slightly higher pump power (red line) the peak is at ∼0.93 GHz. The inset shows the broadband nature the spectra.

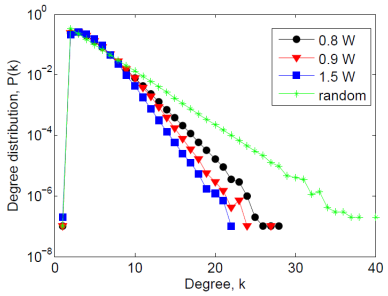

FIG. 2. HVG degree distributions of "raw" intensity time series for various pump powers. For comparison the distribution obtained from Gaussian white noise is also displayed.

successive increments are as likely to have the same sign as the opposite. The fractional Gaussian noise (fGn) is $\mathbf{W}^{\mathcal{H}}(t) = \mathbf{B}^{\mathcal{H}}(t+1) - \mathbf{B}^{\mathcal{H}}(t)$ (fBm-increments) and with $\mathcal{H} = 0.5$ represents Gaussian white noise.

Figure 2(a) displays the degree distributions $P(k)$ obtained from the "raw" intensity time series below, at, and above the transition to turbulence, and also from Gaussian white noise. These distributions can be fitted to $\exp(-\lambda k)$ with $\lambda = 0.59$, 0.69 and 0.75 for pump power 0.8 W (before), 0.9 W (at) and 1.5 W (after the transition). By comparing these λ values with those obtained from fBm generated with different H values [10], and considering the same scaling region ($3 \leq k \leq 20$), we infer the Hurst exponent to be $\mathcal{H} = 0.3$, 0.5 and $\tilde{0}.6 - 0.7$ for 0.8 W, 0.9 W and 1.5 W, respectively. Thus, according to the conjecture proposed in Ref. [9] the dynamics changes from anti-persistent (before the transition) to persistent (after the transition). At the transition, the value of λ is comparable to the one found for fBm with $\mathcal{H} = 0.5$ that corresponds to pure Brownian motion.

In contrast, if we first threshold the raw data and keep only the intensity peaks that are higher than a certain threshold (as in [7], we use a threshold equal to the intensity mean value plus two standard deviations) we find that the thresholded data has very different properties, with λ values being consistent with those found for fractional Gaussian noises (fGn) with $\lambda = 0.403$ ($\mathcal{H} = 0.5$) before the transition, $\lambda = 0.43$ ($\mathcal{H} = 0.7$) at the transition and $\lambda = 0.395$ ($\mathcal{H}$ $0.4 - 0.5$) after the transition. At the transition $\lambda = 0.43$, indicates a persistent fractional Gaussian noise, while all other λ values are very close to the λ value found for Gaussian white noise ($\lambda = 0.405$).

This effect of the threshold resembles the threshold sensitivity found in certain chaotic systems, where varying the threshold can lead from clustering to repelling of extreme events, or vice versa [13].

While this approach for analyzing the persistence properties of a time series is straightforwards to apply, it is limited to the fit of $P(k)$ to an exponential, and therefore, detailed information about the shape of $P(k)$ is lost. It also has the drawback that λ depends on the scaling region. An alternative approach is based on the entropy, $S[P]$, and the Fisher information, $F[P]$ [14] of the HVG degree distribution, $P(k)$. In this way, each time series is represented as a dot in the $S[P] \times F[P]$ plane [15], and a "trajectory" is obtained as the pump power is increased, which captures changes in the dynamics.

In Fig. 3 the results of the analysis of the raw and the thresholded intensity data are compared to synthetic data (fBm and fGn). We note that the two empirical datasets are located very close to the noise "frontier" described in [10]. In agreement to what it was previously inferred with the λ conjecture, the raw data is located very close to the fBm processes; at the transition is close to the ordinary Brownian motion, and after the transition the correlation strength increases with the pump power until 1.4 W, and slightly decreases for 1.5 W. The intensity peaks above the transition, also in good agreement with the λ method, is very well represented by the fGn processes. The transition point (0.9 W) has the lowest $S[P]$ and the lowest $F[P]$, and thus, is a return point of the trajectory in the $S[P] \times F[P]$ plane.

Figure 4 displays $S[P]$ and $F[P]$ vs. the laser pump power (which was indicated in color code in Fig. 3), and it can noticed that, in the raw data, $S[P]$ and $F[P]$ vary gradually, while in the thresholded data, both drop sharply and then rise gradually.

For the thresholded data above the transition, both, the $S[P] \times F[P]$ plane and the fitting of the λ parameter show consistency with fGn, however there is a difference in relation to the strength of the correlations and the inferred $\mathcal{H}$ value. The $S[P] \times F[P]$ plane locates the transition point slightly below the fGn range (indicated with triagles), while the fitting of λ indicates similarity with a persistent fGn ($\mathcal{H} = 0.7$). This difference could be due to the high sensitivity of the fitting parameter to the selection of the scaling zone, or to the finite length of the thresholded time series (while all the raw time series have 5×10^7 data points, the thresholded time series have $10^4 - 10^5$, depending on the pump power [7]).

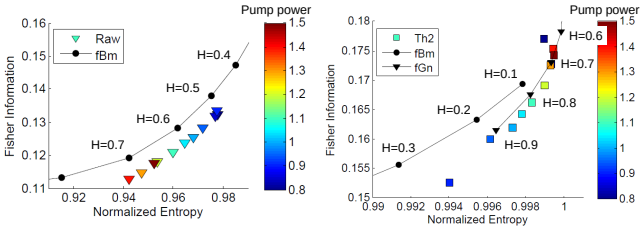

FIG. 3. The HVG entropy, S, and Fisher information, F, computed from the empirical intensity time series (left: raw data, right: thresholded intensity peaks) are compared with synthetic data. The entropy is normalized to the entropy of Gaussian white noise. For the empirical data, the color code indicates the laser pump power; for the synthetic data (black symbols) the Hurst exponent, H, is indicated.

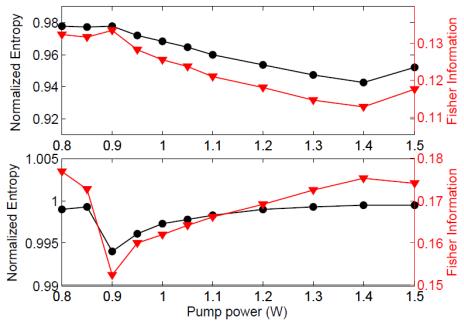

FIG. 4. The HVG entropy, S (circles), and the Fisher information, F (triangles), computed from the raw intensity time series (top) and from the thresholded intensity peaks (bottom) are plotted vs. the pump power. It can be observed that in the raw intensity data, S and F capture a gradual variation of statistical properties of the intensity dynamics during the transition; in contrast, when computed from the thresholded data, S and F uncover a sharp transition.

To analyze long-range temporal correlations we apply to the raw intensity data symbolic ordinal analysis [16–19]. This method is based in transforming a time series into a sequence of symbols that are defined by a rule that takes into account the *relative temporal ordering* among D values in the time series, but not the values themselves.

To fix the ideas, considering pairs of consecutive intensity values, $I_i < I_{i+1}$ gives symbol '01', while $I_i > I_{i+1}$ gives '10'. If we consider $D = 3$ values, there are 6 possible symbols: $I_i < I_{i+1} < I_{i+2}$ gives '012', $I_i < I_{i+2} < I_{i+1}$ gives '021', etc. Considering D values, there are $D!$ possible symbols (known as ordinal patterns) and by computing their probabilities we can detect temporal correlations: if all the symbols are equally probable we can infer that there is no temporal ordering in the sequence, while on the contrary, more probable and less probable symbols uncover the presence of preferred and unfavored order relations. Ordinal analysis was also used in [7] to investigate the intensity dynamics and the results were consistent with those obtained with HVG analysis.

Here we apply ordinal analysis to the raw intensity time series, and, as in [7], we use a lag to uncover order relations among three values $(I_i, I_{i+\tau}, I_{i+2\tau})$, where τ is an integer that gives an effective sampling time of τdt. In this way, each symbol encodes information about the intensity evolution during an interval of $3\tau dt$.

The analysis of the ordinal probabilities vs. τ, shown in Fig. 5, reveals that below and above the transition there are no long-range correlations, as in panels 5(a) and 5(d), for τ large enough, the six patterns are equally probable. In contrast, at the transition [Fig. 5(b)] the pattern probabilities oscillate regularly with periodicity of about 2.5 ns. For a pump power slightly above the transition, Fig. 5(c), there are also regular oscillations of the probabilities with τ, but the oscillations are of smaller amplitude.

Let us next show that these oscillations are captured by a remarkably simple model: a phase equation describing an stochastic limit cycle.

Considering that the polar coordinates of a particle moving in a limit cycle trajectory are $a(t)e^{i\phi t}$ and neglecting the amplitude variations, the dynamics is described by a single rate equation for the phase:

$$d\phi/dt = \omega_0 + f(\phi, t) + \zeta(t), \qquad (1)$$

where ω_0 is the angular rotation frequency, $f(\phi, t)$ is a 2π periodic function $[f(\phi, t) = f(\phi + 2\pi, t)]$ that represents the variability of the instantaneous frequency, and ζ represents stochastic fluctuations.

By stroboscopic sampling every time interval ΔT, the limit cycle evolution is described by a circle map [20]:

$$\phi(t + \Delta T) = \phi(t) + \omega_0 \Delta T + F(\phi, t) + \xi(t), \qquad (2)$$

where $F(\phi, t)$ is a 2π periodic function that represents the phase accumulated over the time interval ΔT, due to the variability of the instantaneous frequency, and ξ represents the influence of the stochastic term. Assuming $F(\phi, t) = K \sin(\phi)$ gives

$$\phi_{i+1} = \phi_i + \epsilon\rho + (K/2\pi)\sin(2\pi\phi_i) + D\xi_i. \qquad (3)$$

where $\phi_i = \phi(t)$, $\phi_{i+1} = \phi(t + \Delta T)$, $\rho = \nu_0 \Delta T$ with $\nu_0 = \omega_0/2\pi$. We also include a parameter $\epsilon = \pm 1$ that determines the direction of the rotation (anticlockwise or clockwise). In the following we assume that ξ_i a Gaussian white noise and D is the noise strength.

Next, we apply ordinal analysis to phase increments, $\Delta\phi_i = \phi_i - \phi_{i-1}$, generated from iterations of this map. We keep constant the strength of the nonlinearity, K, and the strength of the noise, D, and vary ρ as control parameter. We chose ρ because it is proportional to the stroboscopic sampling time, ΔT, which is analogous, in the experimental situation, to the effective sampling time of the laser intensity, τdt, used to define ordinal patterns from lagged intensity values.

For appropriated values of K and D we find that the circle map gives a set of ordinal probabilities that are in remarkable agreement with those computed from the laser data at the transition.

Figure 6 allows a precise comparison: panels (a) and (b) display in detail the oscillatory behavior of the probabilities with the effective sampling time of the intensity time series, while panels (c) and (d) display the probabilities computed from iterations of the circle map. We observe an excellent agreement as the same hierarchical structure (more/less probable patterns) and clustered structure (pairs of patterns with the same probability) are seen when comparing the empirical and the synthetic data. We note that the ordinal probabilities at the transition, Fig. 6(a), are reproduced by the iterations of the circle map with $\epsilon = 1$, Fig. 6(c), while slightly above the transition, Fig. 6(b), with $\epsilon = -1$, Fig. 6(d). This suggests that immediately after the transition there is a change of rotation.

Contrasting similar situations in Figs. 6(a) and 6(c), we observe that $\rho = 1$ in the circle map data corresponds to $\tau = 2.5$ ns in the laser data (as indicated with arrows). Because $\rho = \nu_0 \tau$, using $\rho = 1$ and $\tau = 2.5$ ns we can estimate the frequency of the rotation in the limit cycle as $\nu_0 = 1/\tau = 0.4$ GHz, in agreement with the narrow peak seen in the spectrum in Fig. 1. Also comparing similar situations immediately after the transition, in Figs. 6(b) and 6(d), we observe that $\rho = 2$ in the circle map data corresponds to $\tau = 4.3$ ns in the laser data (as indicated with arrows). The same argument gives $\nu_0 = 2/\tau = 0.46$ GHz, and the spectrum in Fig. 1 we see the peak at about 0.93 GHz, which is consistent with $2\nu_0$.

The agreement found is unexpected because, as shown in the inset of Fig. 1, the spectrum is extremely broad and thus, it is surprising to find that, in the symbolic representation, the intensity temporal dynamics is described by an stochastic limit cycle with rotation frequency ν_0. It is worth noticing that statistical properties of the intensity values are not described by the statistics of the phase increments, $\Delta\phi_i = \phi_i - \phi_{i-1}$, which take both, positive and negative values.

To summarize, we have applied various data analysis tools to characterize persistence and temporal correlations in the intensity dynamics of a fiber laser. To characterize the persistence, intensity time series (raw and thresholded data) were transformed to graphs through the horizontal visibility algorithm and then compared with well-known stochastic processes, fractional Brownian motions (fBm) and fractional Gaussian noises (fGn).

Two different techniques that use the graph degree distribution (fitting the distribution to an exponential, and computing, from the degree distribution, the Shannon entropy and the Fisher information) gave consistent results, with the raw intensity data being consistent with fBm processes, and the thresholded data, with fGn. At the transition the raw data is well represented by fBm

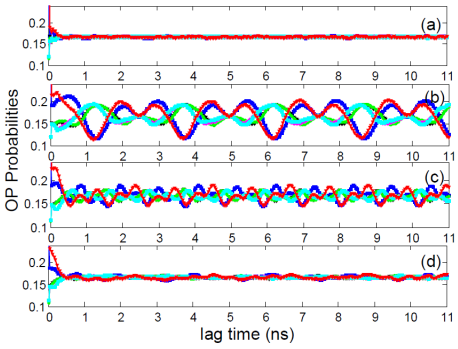

FIG. 5. Probabilities of the ordinal patterns computed from the laser intensity vs. the sampling time. The pump power is as in Fig. 1: (a) 0.8 W, (b) 0.9 W, (c) 0.95 W and (d) 1.0 W.

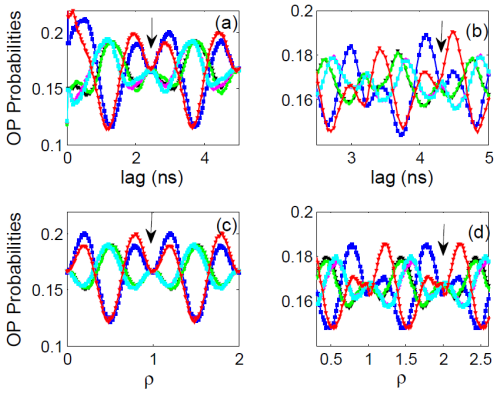

FIG. 6. Comparison of the ordinal probabilities computed from empirical data, panels (a) and (b), and from synthetic data, panels (c) and (d). In (a) and (b), the probabilities are computed from the laser intensity time-series and the horizontal axis is the sampling time; the laser operating condition is (a) at the transition and (b) slightly above the transition (pump power 0.9 W and 0.95 W, respectively). In panels (c) and (d), the probabilities are computed from data generated by iterating the circle map, Eq. (3), and the horizontal axis is the map parameter, ρ; the other parameters are (c) $K = 0.1$, $D = 0.02$, $\epsilon = 1$; (d) $K = 0.25$, $D = 0.075$, $\epsilon = -1$.

with Hurst exponent $\mathcal{H} = 0.5$, which corresponds to pure Brownian motion. Above the transition, both methods find persistent processes (fBm with $\mathcal{H} > 0.5$). For the thresholded data above the transition, both methods show consistency with fGn.

We have also demonstrated that at the transition, temporal correlations can be precisely represented by a surprisingly simple model: a circle map. The physics underlying the emergence of stochastic periodicity at the transition could be mode locking, and merits further investigation. The analysis tools proposed here can be applied to the output signals of other systems that undergo similar transitions to turbulent behavior [21, 22].

We gratefully acknowledge Prof. S. K. Turitsyn (Aston University, U.K.) for the permission to use the datasets

analysed in [7]. L. C. acknowledges support from Brazilian agencies FAPEMIG (Project Number: APQ-03664-16), CNPq and CAPES. C. M. acknowledges partial support from Spanish MINECO (FIS2015-66503-C3-2-P) and from the program ICREA ACADEMIA of Generalitat de Catalunya.

* cristina.masoller@upc.edu

[1] S. K. Turitsyn, S. A. Babin, A. E. El-Taher, P. Harper, D. V. Churkin, S. I. Kablukov, J. D. Ania-Castanon, V. Karalekas, and E. V. Podivilov, Nat. Photonics **4**, 231–235 (2010).

[2] S.V. Sergeyev, H. Kbashi, N. Tarasov, Yu. Loiko, and S.A. Kolpakov, Phys. Rev. Lett. **118**, 033904 (2017).

[3] K. Krupa, K. Nithyanandan, U. Andral, P. Tchofo-Dinda, and P. Grelu, Phys. Rev. Lett. **118**, 243901 (2017).

[4] E. G. Turitsyna, S. V. Smirnov, S. Sugavanam, N. Tarasov, X. Shu, S. A. Babin, E. V. Podivilov, D. V. Churkin, G. E. Falkovich, and S. K. Turitsyn, Nat. Photonics **7**, 783 (2013).

[5] D. V. Churkin, S. Sugavanam, N. Tarasov, S. Khorev, S. V. Smirnov, S.M. Kobtsev, and S. K. Turitsyn, Nat. Commun. 6, 7004 (2015).

[6] A. K. Chattopadhyay, D. Nasiev, S. Sugavanam, N. Tarasov, and D. V. Churkin, Sci. Rep. **6**, 28492 (2016).

[7] A. Aragoneses, L. Carpi, N. Tarasov, D. V. Churkin, M. C. Torrent, C. Masoller, and S. K. Turitsyn, Phys. Rev. Lett. **116**, 033902 (2016).

[8] B. Luque, L. Lacasa, J. Luque, and F. J. Ballesteros, Phys. Rev. E **80**, 046103 (2009).

[9] L. Lacasa and R. Toral, Phys. Rev. E **82**, 036120 (2010).

[10] M. G. Ravetti, L. C. Carpi, B. Goncalves, A. C. Frery, and O. A. Rosso, PlosONE **9**, e108004 (2014).

[11] J. F. Muzy, E. Bacry, and A. Arneodo, Phys. Rev. Lett. **67**, 3515 (1991).

[12] G. Stolovitzky and K. R. Sreenivasan, Rev. Mod. Phys. **66**, 229 (1994).

[13] T. Schweigler and J. Davidsen. Phys. Rev. E **84**, 016202 (2011).

[14] If $P = [p_i; i = 1, ..., M]$ is a discrete probability distribution, with M being the number of possible states, the Shannon entropy and the Fisher information are calculated as $S[P] = -\sum_{i=1}^{M} p_i \ln p_i$ and $F[P] = F_0 \sum_{i=1}^{M-1} \left[p_{i+1}^{1/2} - p_i^{1/2}\right]^2$ with F_0 a normalization constant [10].

[15] C. Vignat and J. F. Bercher, Phys. Lett. A. **312**, 27 (2003).

[16] C. Bandt and B. Pompe, Phys. Rev. Lett. **88**, 174102 (2002).

[17] M. Zanin, L. Zunino, O. A. Rosso, and D. Papo, Entropy 14, 1553 (2012).

[18] J. M. Amigo, K. Keller, and J. Kurths, Eur. Phys. J. Spec. Top. 222, 241 (2013).

[19] X. Sun, M. Small, Y. Zhao and X. Xue, Chaos 24 024402 (2014).

[20] A. Pikovsky, M. Rosenblum, and J. Kurths, *Synchronization: A Universal Concept in Nonlinear Sciences* (Cambridge University Press, Cambridge, U.K., 2001).

[21] D. Pierangeli et al., Phys. Rev. Lett. 117, 183902 (2016).

[22] I. R. R. Gonzalez, B. C. Lima, P. I. R. Pincheira, A. A. Brum, A. M. S. Macedo, G. L. Vasconcelos, L. D. Menezes, E. P. Raposo, A. S. L. Gomes, and R. Kashyap, Nat. Commun. 8, 15731 (2017).